PAPER • OPEN ACCESS

A drift-diffusion simulation model for organic field effect transistors: on the importance of the Gaussian density of states and traps

To cite this article: Mohammed Darwish and Alessio Gagliardi 2020 *J. Phys. D: Appl. Phys.* **53** 105102

View the article online for updates and enhancements.

Recent citations

IOP ebooks™

Bringing together innovative digital publishing with leading authors from the global scientific community.

Start exploring the collection–download the first chapter of every title for free.

A drift-diffusion simulation model for organic field effect transistors: on the importance of the Gaussian density of states and traps

Mohammed Darwish and **Alessio Gagliardi**

Department of Electrical and Computer Engineering, Technical University of Munich, Munich 80333, Germany

E-mail: mohammed.darwish@tum.de

CrossMark

Abstract

The nature of charge transport in organic materials depends on several important aspects, such as the description of the density of states, and the charge mobility model. Therefore specific models describing electronic properties of organic semiconductors must be considered. We have used an organic based drift-diffusion model for the electrical characterization of organic field effect transistors (OFETs) utilizing either small molecules or polymers. Furthermore, the effect of interface traps, bulk traps, and fixed charges on transistor characteristics are included and investigated. Finally, simulation results are compared to experimental measurements, and conclusions are drawn out in terms of transistor performance parameters including threshold voltages, and field-dependent mobilities.

S Supplementary material for this article is available online

(Some figures may appear in colour only in the online journal)

1. Introduction

Organic materials and devices have been at the forefront of the research community in recent years due to their flexible properties, as well as the large scale roll-to-roll cheaper fabrication procedures. Eventhough, inorganic semiconductors have been (and still are to a large extent) the go-to materials for today's electronic industry, research have come a long way in improving performance measures of organic based devices since their first introduction. Such devices include organic-solar cells (OSCs) [1–3], and light emitting diodes (OLEDs) [4–7]. The latter one especially made a breakthrough on the commercial scale for display applications (i.e. mobile phones

and the recently introduced OLED TVs). Organic field-effect transistors (OFETs) (the main focus of this work) have also been (and still are) investigated heavily [8–11]. In a recent review published by Paterson and co-workers [12], the authors provide a graphic showing the progress acheived in OFET mobilities over the past 30 years. According to this graphic, both p- and n-type mobilities have reached up to $20 \, \text{cm}^2 \, \text{V}^{-1} \, \text{s}^{-1}$ and $10 \, \text{cm}^2 \, \text{V}^{-1} \, \text{s}^{-1}$, respectively. This definitely spells significant improvements, but they go on to say that these values do not paint the entire picture and in reality there is what they refer to as a 'mobility hype'. This hype points towards that there has been an overestimation in OFET mobilities, as a consequence of extracting mobilities from characteristics (i.e. transfer and output) that show non-ideal behaviour. This non-ideality is depicted as a 'double slope', leading to overestimated mobilities from the steeper portion of the transfer characteristics. Contact resistance is identified as the main

cause for the resulting non-idealities [13–16]. Nevertheless, even with the presence of this mobility hype, there is no denying the fact that improvements in OFET mobilities have been made [12]. Advancements in OFETs is also aided with the different types of materials available to choose from [17], for both hole and electron conduction. This also, theoretically, allows organic semiconductors the possibility to enter the digital market (i.e. complementary technologies) [18–20]. More recently, research has gone into investigating blend based OFETs, incorporating both small molecules and polymers. This is particularly interesting as we can take advantage of what both types of materials have to offer, the high mobility of small molecules and the easier processability of polymers. Mobilities ranging up to $13 \, \text{cm}^2 \, \text{V}^{-1} \, \text{s}^{-1}$ have been reported [21–24]. There is not alot available on blends in the literature to date, but with the the early promise blends have shown, more interest will certainly focus on that front.

The working principle of a FET is always the same, regardless of the active material used for the channel region. However, the underlying physics governing charge transport is different between organic and inorganic materials. For the latter, charge transport occurs via coherent Bloch waves. In contrast, for the former, it is through hopping from one site to another within a varying energetic landscape, owing to individual molecules being bound together through weak Van der Waals interactions. Therefore, charge transport occurs through hopping between localized states. This hopping mechanism is appropriately described by the Gaussian disorder model (GDM) [25]. These energetic sites follow a random distribution which is described by a Gaussian function in the vicinity of an energy level of interest (i.e. highest or lowest occupied molecular orbitals (HOMO or LUMO) respectively). The width of this function is referred to as the energetic disorder. Such disorder is found in both small molecules and polymers, and is more pronounced in the latter. Multiple theoretical models have been proposed to describe the hopping of charges, namely: (1) nearest neighbour hopping (NNH), (2) variable range hopping (VRH), (3) the transport energy model (TE), and (4) multiple trap and release model (MTR). Motion of charges described by any of these models does not only depend on the electric field but also the temperature. A more detailed overview can be found here [26].

This hopping mechanism is one of several forms of transport used to explain the movement of charges in organic materials. These also include band and polaron transport. Two important requirements need to be achieved for band transport to occur, which are the growth of high quality crystals, and the observation of a negative temperature dependence of the mobility. This dependence has been previously observed in Rubrene FETs by Podzorov *et al* [27, 28]. The review by Hasegawa and Takeya [29] further highlights the significance of fabricating high quality single crystals to achieve high charge mobilities. On the other hand, polaron transport accounts for polarizations, which is a common occurence in organic materials. If a charge is present on a site for a long enough time, it starts to polarize the surrounding environment. The initial charge and the resulting polarization then

propagate (together) within the material known as a polaron. As Horowitz thoroughly explains in [30], there can be different types of polarizations (i.e. electronic, molecular, and lattice) depending on the residence time of a charge on a specific site. A comparison between the different charge transport theories have been addressed, for example see Stallinga [31] and Troisi [32].

Charge transport in organic semiconductors is a much more complex process, therefore careful considerations need to be taken into account for the description of the sub-models used and their parameterizations in any drift-diffusion (DD) simulation. That includes a correct description of the density of states (DOS), the mobiltiy model, and the effect of charge trapping. More importantly, a connection between these models and what actually occurs within organic materials needs to be established, to justify their usability. This allows for the appropriate characterization of organic based devices and subsequent comparison and validation with experimental measurements. The paper is outlined as follows: in section 2, we present theory behind the DD simulation and go through the sub-models used for our investigations. Section 3 will present the results, extracting all important performance measures (i.e. mobilites, threshold voltages) and drawing out a comparison with experimental measurements. Finally, in section 4, we end with our concluding remarks.

2. The drift-diffusion model

The drift-diffusion model involves solving a set of equations, within the finite element method using the the commercial software TiberCad. This DD model has been previously used investigating both inorganic and organic based devices for different applications [33–40]. Furthermore, it has also been used for the investigation of charge carrier mobility unbalance in organic solar cells [41], as well as alongside circuit level modelling for identifying low conductive regions in organic thin films as a result of charge carrier trapping [42]. In this study we start by creating a structure, then a corresponding mesh is generated consisting of many elements, for which the DD equations are applied to and solved. We will be considering a 2-dimensional (2D) bottom gate-bottom contact (BG-BC) structure. Both the 2D device and the meshed representation are shown in figure 1.

The main equations of the DD model are the Poisson and continuity equations given by:

$$\nabla \cdot (\varepsilon \nabla \varphi) = e(p - n + N_D - N_A + p_t - n_t) = \rho \quad (1)$$

$$\nabla \cdot j_n = \nabla \cdot (\mu_n n \nabla \varphi_n) = -R + G \quad (2)$$

$$\nabla \cdot j_p = \nabla \cdot (\mu_p p \nabla \varphi_p) = R - G, \quad (3)$$

where ε is the permittivity, e the electronic charge, φ the electric potential, n and p the electron and hole mobile charge densities, N_D and N_A the donor and acceptor concentrations respectively. The terms p_t, n_t represent trap densities, and finally ρ is the charge density. In (2) and (3), μ_n and μ_p are the charge mobilites, G and R are the generation and
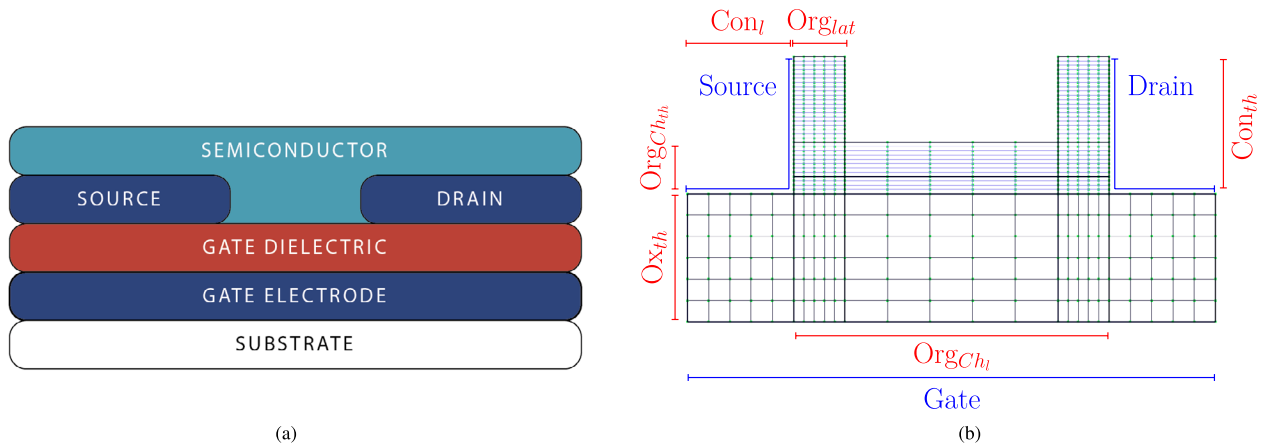
Figure 1. A 2D illustration of a bottom gate-bottom contact, in both (a) device and the corresponding (b) meshed representations. Dimension labels are illustrated and further explained in detail in section 3.4. (a) Bottom gate-bottom contact (BG-BC). (b) Mesh representation (BG-BC)).

recombination terms. In our transistor analysis both generation and recombination will not be considered. The presented work focuses on unipolar devices, hence the reasoning behind not considering the latter. We start by sweeping on the gate voltage, followed by a sweep on the drain voltage at each gate. During this process the DD equations are solved self consistently and the drain current calculated. In the following subsections, we will go through (in more detail) the different physical models used for our transistor analysis.

2.1. Gaussian density of states (GDOS)

As it was stated before, charge transport in organic semiconductors relies on a a hopping mechanism through a random distribution of localized states. In order to have an appropriate description for this charge hopping, the DOS is best described by a Gaussian function. This function is expressed as

$$g(E) = \frac{N_0}{\sigma\sqrt{2\pi}} \exp\left(-\frac{E^2}{2\sigma^2}\right), \tag{4}$$

where N_0 is the site density, E the energy, and σ the energetic disorder respectively. Energetic disorder in organic semiconductors typically lies in the range between 30 meV and 100 meV [43, 44], and it relies on the morphology of the material. That is why polymers suffer from higher disorder compared to small molecules. Going from low to high disorder leads to an increase in the random distribution of sites further away from the transport level, as a consequence some of these sites might act as trap states affecting overall charge transport. Moreover, it has been shown that charge mobilites depend on the applied field, carrier density, and temperature (more on this will be discussed in sub-section (C)). The dependence of the mobility on the latter two is affected by the DOS. Therefore, it is crucial to have a correct description of the DOS and the appropriate amount of disorder depending on the material chosen.

2.2. The trap model

Charge carrier trapping in organic semiconductors is one of the major factors affecting device performance. Depending on the energy associated with a trap state (i.e. how far it is inside the band gap), this can have different effects on device operations such as degrading mobilites [27, 45, 46], causing hysteresis [47], and leading to threshold voltage shifts [48, 49]. Stability over extended periods of time is also a major issue in organic devices, more specifically the ones incorporating n-type materials as the active region. This is one of the reasons why complementary logic based on organics has been proven difficult to achieve. It is imperative to include traps in any DD simulation, and their effects could be seen from the transfer characteristics of an OFET. Traps in our DD simulations are modelled as follows:

(i) A neutral trap that becomes negatively charged when an electron is trapped

$$n_t = \frac{N_t}{1 + \exp\left(\frac{(E_c - E_{t_n}) - E_{F,n}}{k_b T}\right)}. \tag{5}$$

(ii) A neutral trap that becomes positively charged when an hole is trapped

$$p_t = \frac{N_t}{1 + \exp\left(-\frac{(E_v + E_{t_p}) - E_{F,p}}{k_b T}\right)}. \tag{6}$$

(iii) Fixed charges where the density is simply defined. They can be either positive or negative.

In (5) and (6), N_t denotes the density of traps, E_{t_n} and E_{t_p} the electron or hole trap energy level, $E_{F,n}$ and $E_{F,p}$ are the quasi-fermi energies, k_b the Boltzmann constant, and T the temperature respectively. The trap level can be taken with reference to the conduction or valence bands (i.e. E_c or E_v).

The above mentioned models (and their subsequent effect on charge transport) have been used extensively for the

J. Phys. D: Appl. Phys. **53** (2020) 105102

M Darwish and A Gagliardi

investigation of inorganic materials and devices. In order to justify their usage towards investigating charge transport in organics, they must be able to represent the physical meaning of certain phenomena (or events) that occur within organic materials and devices. One of these events is the presence of dipoles, more specially interface dipoles. Dipoles exist as a result of inhomogeneous distribution of charges at a surface [50]. Such dipoles can occur at organic–organic [51, 52], organic-metal interfaces [53–55], and even with dielectric interfaces [56]. Infact, self-assembled monolayers (SAMs) have been previously used to intentionally induce interface dipoles between the organic and dielectric materials, to influence the electrical characteristics of OFETs. As a result, controlling of charge densities leading improved field effect mobilities, as well as threshold voltage shifts have been observed [57–59]. A presence of a dipole causes a shift in the potential between two different interfaces (or surfaces). This shift is expressed as

$$\Delta_d = \frac{q m_d cos\theta}{A_d \varepsilon}, \tag{7}$$

where q is the electronic charge, m_d is the electric dipole moment (given in units of debye and depends on the distance between the positive and negative charges), θ is the angle of the dipole with respect to the surface, A_d is the area of the surface charges, and lastly ε is the dipole layer's dielectric constant. Similarly, fixed charges represent a surface area of charges present at an interface and through coulomb attraction, charges of the opposite sign are situated on the other side. Hence, this would be expressed as

$$\Delta_d = \frac{q}{A_d \varepsilon}. \tag{8}$$

Both (7) and (8) are almost identical with the exception of the angle θ, allowing us to use a model of fixed charges to represent the effect of dipoles in our simulations. This assumption is valid if the distance between the separate charges is within a fraction of a nanometer. In the following section, we show how the fixed charges does indeed affect the threshold voltage and subsequently the field-effect mobility, therefore allowing us to account for interface dipole effects.

A similar connection can be achieved in regards to the modelling of trap states in our DD simulations. It is already quite obvious that the mentioned trap models can be used to describe defects withing organic materials. Such defects can be structural, energetic, or a combination both. However, these trap models can also be used to account for redox states. Organic materials have been shown to go through redox reactions [60]. These reaction involves transfer of electrons from (i.e. oxidation) or to (i.e. reduction) the host material. Organic electrochemical transistors (OECTs) that rely on transitioning between redox states, have been under investigation for biological applications [61]. According to a recent review on OECTs by Zeglio and Inganäs [62], changes in redox states of organic materials are associated with energy levels formed inside the band gap. These intermediate levels act as doping or de-doping centers when the device is operated under an external potential. This process can also be interpreted as

charge carrier trapping and de-trapping, and our DD trap models can be used to account for these effects as well.

Therefore, if simulated traps are intended to represent defects, then (5) and (6) stand. On the other hand, if they were to represent redox reactions, in this case both E_{t_n} and E_{t_p} in (5) and (6) are simply replaced with E_{redox}. Furthermore, N_t would then represent the molecules (i.e. they are either reduced or oxidized). This effectively means that N_t has to be equal to N_0 from (4). Nevertheless, it might be possible that N_t be somewhat higher or lower. Equations (5) and (6) represent a classical description of the density. Conversely, in organics the description of the density is of a quantum mechanical nature. This is linked to the delocalization of the wavefunction, where molecules can be charged by a fractional charge (i.e. only a fraction of the quantum state is localized on a specific molecule). As a result, the density N_t can have values which are both larger or smaller than the value of the molecular density N_0. In our simulation process, we will start by defining single trap levels, but if needed it is also possible to define a distribution of trap states with the Gaussian function from (4).

2.3. The mobility model

Describing how charges move within a transistor channel is an integral part of any DD simulation, and there are multiple models available in the TiberCad tool to choose from. Specific to organic semiconductors there are two models that are usually used for such investigations. We will present an overview on both models, and how the decision is taken on which one to use moving forward with the simulations.

2.3.1. The Pasveer mobility. This mobility model which was developed by Pasveer *et al* [63, 64], is obtained as a parametrical fit of numerical solutions of a system of master equations implementing the Miller–Abrahams [65] hopping model between localized states with a Gaussian energy distribution. The model takes into account the dependence of the mobility on the temperature, charge density, and electric field:

$$\mu(T, \rho, F) = \mu(T, \rho) f(T, F). \tag{9}$$

The Pasveer mobility has been used to fit experimental results for different semiconducting polymers [37, 38, 66]. Nevertheless, the authors also state that the above parameterization starts to breakdown at high electric field, hence a cutoff has been defined where beyond it the breakdown occurs [38], and is given by

$$F > \frac{2\sigma}{ea}. \tag{10}$$

2.3.2. The Poole–Frenkel mobility. According to Pasveer, at high electric field and beyond the cut-off mentioned above, the mobility starts to follow the Poole–Frenkel law (PF) [67]. The PF mobility model is a widely known and used one in the literature for investigating charge transport in organic semiconductors [26, 68–70]. According to PF, the mobility is expressed as:

J. Phys. D: Appl. Phys. 53 (2020) 105102

M Darwish and A Gagliardi

Table 1. The different dimension labels used to define the meshed structures and their assigned lengths.

Dimension labels & values	
Oxide thickness (Ox_{th})	Defined by experiment
Channel length (Org_{ch_l})	Defined by experiment
Channel thickness (Org_{ch_th})	10 nm
Organic lateral dimension (Org_{lat})	10 nm
Contact length (Con_l)	50 nm
Contact thickness (Con_{th})	100 nm

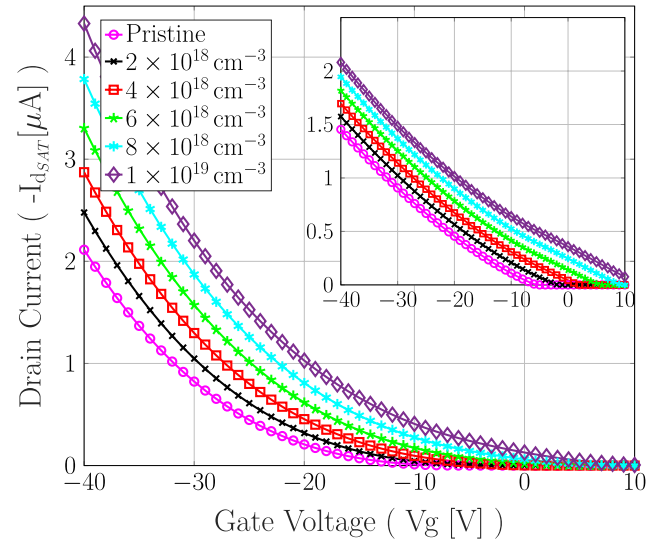$$\mu = \mu_0 \exp\left(-\frac{\Delta - \gamma\sqrt{F}}{kT}\right), \qquad (11)$$

where μ_0 is the zero-field mobility, Δ the zero-field activation energy, γ the Poole–Frenkel constant [71], and F the electric field respectively. This relation specifies that charges can gain the required energy from the applied electric field to overcome potential barriers, as they hop from one site to another, equal to a certain activation energy that is otherwise not provided (or insufficient) thermally. Furthermore, as the mobility depends on both the temperature and applied field, the dependence on the temperature vanishes at the point of $F = (\Delta/\gamma)^2$. At this point, the applied field is equal to the activation energy so that at different temperatures the mobility will always reach the same value [68].

Deciding on which mobility model to use for our DD simulations, depends on several aspects. The PF model better suits small molecules, while the hopping mobility is used for polymers. The numerical solution presented by Pasveer was mainly based on investigating polymers. Furthermore, if the DD model is used to investigate polymer based OFETs, we must first find out where we lie with respect to the cut-off defined by (10). If the electric field is lower then the hopping mobility is chosen, otherwise the PF is then the one used.

2.4. Simulation related remarks

In this sub-section we will point out some simulation related remarks. As mentioned earlier, a BG-BC transistor architecture will be considered. Looking back to figure 1(b), the device is split up into two major regions, the oxide and the organic. The organic region itself is further split up into two, where the top part is the bulk, and the bottom part used to to model interface effects. In regards to the contacts, they are all defined as physical lines (i.e. boundaries) of the device. Bulk representation of the contacts are not taken into account, as they effectively do not change anything in terms of current–voltage characteristics. With this exclusion we are able to gain improvements on simulations times.

In regards to the dimensions, we construct our 2D meshed representation based on the following device dimension labels: the oxide thickness (Ox_{th}), the channel length (Org_{ch_l}), the channel thickness (Org_{ch_th}), the lateral dimension of the organic near the contacts (Org_{lat}), the contact length (Con_l), and lastly the contact thickness (Con_{th}). Only the Ox_{th} and Org_{ch_l} are changed with respect to experimental values,

Figure 2. The effect of fixed charges on the transfer characteristics of an OFET. The square root of the drain current versus the gate voltage ($\sqrt{Id_{SAT}}$ versus V_g) is shown in the inset.

while the rest are pre-defined and always fixed. A summary of these dimension labels are given in table 1 (also shown in figure 1(b)).

Org_{ch_l} was chosen to be 10 nm, as it is well known that charge transport usually occurs within the first few monolayers just above the oxide-organic interface [72, 73]. Furthermore, we did not observe any change in the current–voltage characteristics going beyond this value[1]. For the sake of being consistent, Org_{lat} was chosen to be the same as Org_{ch_l}. Similarly, Con_{th} was also fixed at 100 nm, as increasing the thickness simply increased simulation times without any observed changes in the characteristics.

The PF mobility model has been chosen for our simulations, as we will be presenting results on Pentacene (i.e. small molecule) based OFETs (see section 3). Lastly, both the source and drain are modelled as Schottky contacts (typical for all organic based devices), unless there has been mention of doping near the source/drain. In the latter case the contacts would then be modelled as ohmic.

3. Simulation results

Here, we present a comparison between the DD simulation and experimental results for a BG-BC Pentacene transistor from [74]. Per the fabricated transistor, the channel length is 12 μm. The oxide thickness was not specified from the experiment, hence a typical thickness of 200 nm was chosen. We first start by fitting the transfer characteristics given a set of parameters (i.e. for the models defined in the previous section). Once a good fit is achieved, the output characteristics is simulated using the same model parameters. Before going straight into the comparison, it is important to first understand the behaviour of the transfer characteristics. This is useful especially in the presence of fixed charges and interface (or

---

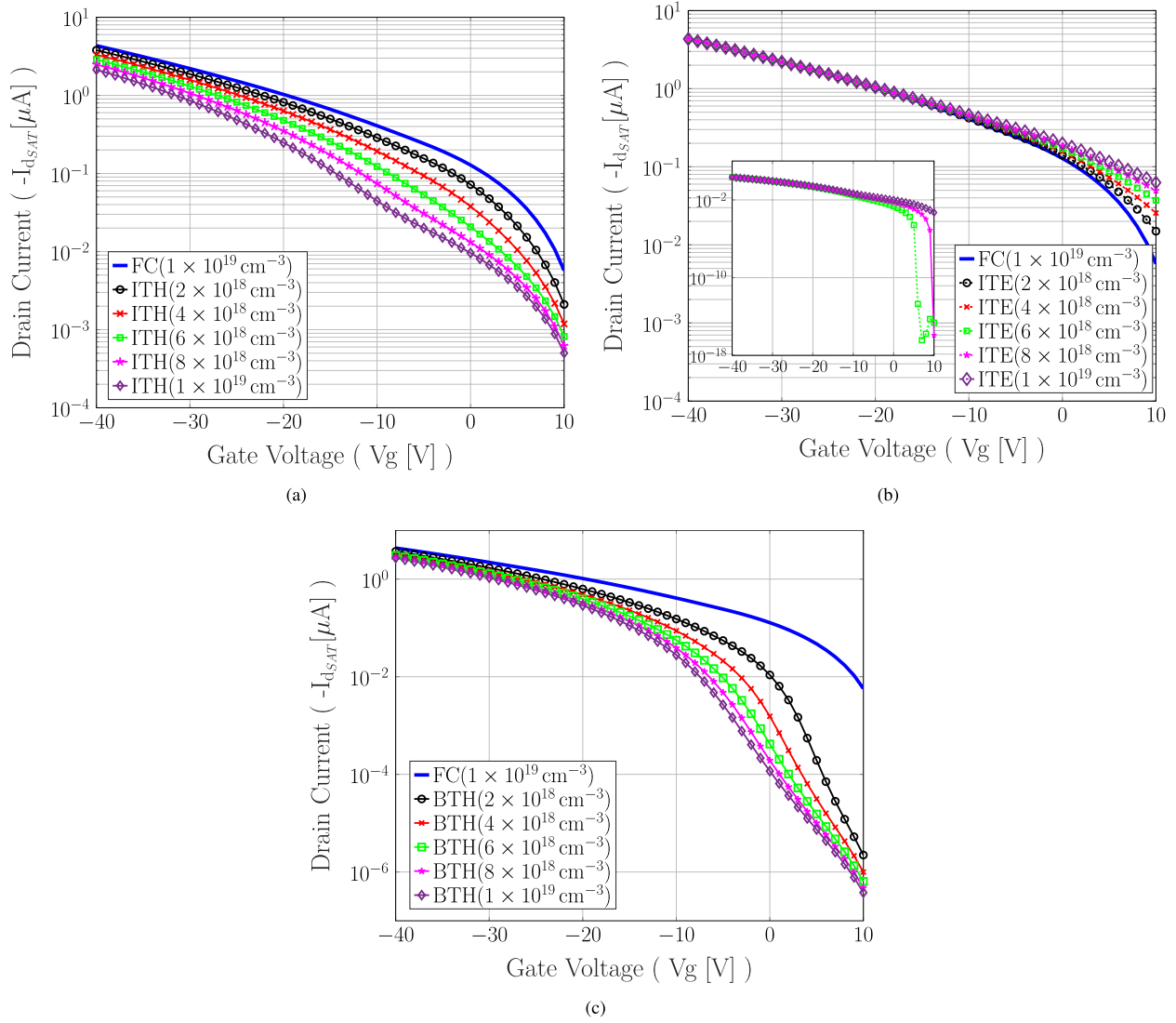[1] These results are not shown here.

Figure 3. Transfer characteristics (at $V_d = -30\,\text{V}$) of a BG-BC OFET under pristine conditions and different concentrations of interface and bulk traps. (a) The effect of positively charged (i.e. hole) interface traps. (b) The effect of negatively charged (i.e. electron) interface traps. (c) The effect of positively charged (i.e. hole) bulk traps.

bulk) traps, where each one has an effect on transistor performance, and such effects can be seen from the transfer curves.

3.1. Trap-free versus fixed charges and interface/bulk traps

We start by investigating the effect of negative fixed charges at the oxide-organic interface (will be referred to from now on as 'FC'). From figure 2, it can be seen that a positive shift in the threshold voltage is induced as we move from a 'pristine' device towards higher concentrations of fixed charges. This behaviour follows the relation:

$$\Delta V_{th} = -\frac{Q_{int}}{C_{ox}}, \tag{12}$$

where ΔV_{th} is the threshold voltage shift, Q_{int} the fixed charge concentration, and C_{ox} the oxide capacitance respectively. This ΔV_{th} is better depicted in the inset of figure 2 by plotting the square root of the drain current ($\sqrt{Id}$), and the threshold

voltage V_{th} is simply the intersection at the x-axis when the current is zero.

Following the inclusion of fixed interface charges, we can now further introduce interface or bulk traps. Traps are regarded neutral if empty, then either positively or negatively charged if occupied by a hole or an electron (will be referred to as 'ITH' and 'ITE' respectively). A single trap level was chosen above the valence band. The effect of both types of charged traps, modelled at the oxide-organic interface, is depicted in figures 3(a) and (b). On one hand, positively charged traps leads to less current drive (i.e. lower drain current and a downward shift in the transfer curve). This is true, as a higher gate voltage is needed to induce more charges in the channel region. Conversely, negatively charged traps lead to a decrease in the inverse sub-threshold slope and as a result a high sub-threshold current is evaluated, eventhough the transistor is operated at high positive gate voltages (i.e. in the off state). At high concentrations of electron traps, the

Table 2. A summarized list of the different parameters used for the DD simulation of a Pentacene BG-BC OFET.

Simulation parameters	
Site density (N_0)	4×10^{19} cm^{-3}
Energetic disorder (σ)	30 meV
μ_0 (PF)	3×10^{-4} cm^2 V^{-1} s^{-1}
F (PF)	3×10^5 V cm^{-1}
n_t/p_t (Interface) energy	0.15 eV
p_t (Bulk) energy	0.3 eV

positive applied gate voltage becomes insufficient to deplete the channel of holes leading to high currents in the off-state. Under negative applied gate voltages no change is observed in the drain current. This is self-evident, as in this voltage regime the channel is filled up with holes as mobile charges and trapped electron concentrations have no effect on the transfer characteristics. Furthermore, the negatively charged traps also lead to ΔV_{th} shifts (inset of figure 3(b)) in the absence of fixed charges. This is not apparent in the main panel of figure 3(b) simply due to the already high presence of fixed charges as a starting point before the interface traps were applied.

Finally, we investigated the effect of positively charged bulk traps (will be referred to as 'BTH') on the transistor performance with a single level above the valence band. As illustrated in figure 3(c), they also have a similar effect to that of the positively charged interface traps. Between bulk and interface traps, the former has a more pronounced effect on the inverse sub-threshold slope. This is a consequence of the bulk traps being located deeper in the band gap. In the supplementary information (stacks.iop.org/JPhysD/53/105102/mmedia), we provide a charge density map projected on our device for the ITH (figure (S1)), ITE (figure (S2)), and BTH (figure (S3)) cases at different densities. From this analysis we were able to show that fixed or trapped charges have their own distinct effects on the transfer characteristics of an organic transistor, but another crucial conclusion from this analysis is that using either fixed charges alone[2] or as a combination with either interface or bulk traps might be insufficient to get a good description of the transfer curves. Possibly a combination between all three of them is required to achieve a good fit with the experimental results.

3.2. Validating experimental data

In this sub-section we aim to present our simulation results and validate them with experimental measurements from [74], by fitting both the transfer and output characteristics of a 12 μm channel Pentacene BG-BC OFET. We start by first achieving the best fit of the transfer characteristics. Once this is completed we use the corresponding parameterizations to simulate the output characteristics. Following the analysis in section 3.1, we are presented with three different scenarios to fit the transfer characteristics starting from a pristine condition, namely:

---

[2] For the shown charge concentrations.

(i) The first scenario includes:

- Negative interface fixed charges, to get the correct V_{th} and hence the slope of the transfer curve in the on-state.
- Positively charged bulk traps, to control the sub-threshold characteristics.
- (If required) Negatively charged interface traps, to have a more precise control over the sub-threshold slope.

(ii) The second scenario includes:

- Negative interface fixed charges, to get the correct V_{th} and hence the slope of the transfer curve in the on-state.
- Positively charged interface traps, to get the appropriate evaluated current across the entire voltage range.
- (If required) Positively charged bulk traps, to control the sub-threshold characteristics.

(iii) The third scenario includes:

- Negatively charged interface traps, to get the correct V_{th} keeping in mind its added effect on the sub-threshold.
- Positively charged bulk traps to adjust the current drive accordingly.

From here onwards we will refer to the three scenarios mentioned above in the same order as SC1, SC2, and SC3 respectively. Simulation parameters used to describe the above scenarios (i.e. fixed an trap concentrations) will be adjusted accordingly to reach the best fit of the transfer characteristics. All other parameters are summarized in table 2. From table 2, all values referring to the μ_0, and interface or bulk trap energies are taken as input from the analysis carried out in [74]. These three parameters will also be carefully adjusted, if it is needed to do so, for the fitting process. The site density N_0, σ, and F are kept fixed.

All three scenarios were considered carefully. And within each one different concentrations for the fixed charges, interface and bulk traps (as well as their energy level) were investigated. It would be difficult to present all these results as we went through numerous parameter sets to achieve the best fit. Out of the three scenarios, we could not reproduce the transfer characteristics with SC3. Using SC1 or SC2, we managed to reproduce an almost perfect fit but only within a specific gate voltage range (between the off-state and up to -20 V of the applied gate voltage). The SC1 and SC2 fits are shown in figure 4, both on the linear and logarithmic scales. Beyond the -20 V mark both SC1 and SC2 drift away from the experimental measurement. By re-adjusting any (or all) of the three parameters within either SC1 or SC2, we were only able to fit the lower part of the transfer curve. This included different trap concentrations as well as their energy level within the band gap. Moreover, applying a GDOS in describing the trap energy as opposed to a single level definition did not bring us closer to a better fit. The only way we were able to fit the upper part of the transfer curve was actually using a fourth and different scenario which involved only the presence of FC
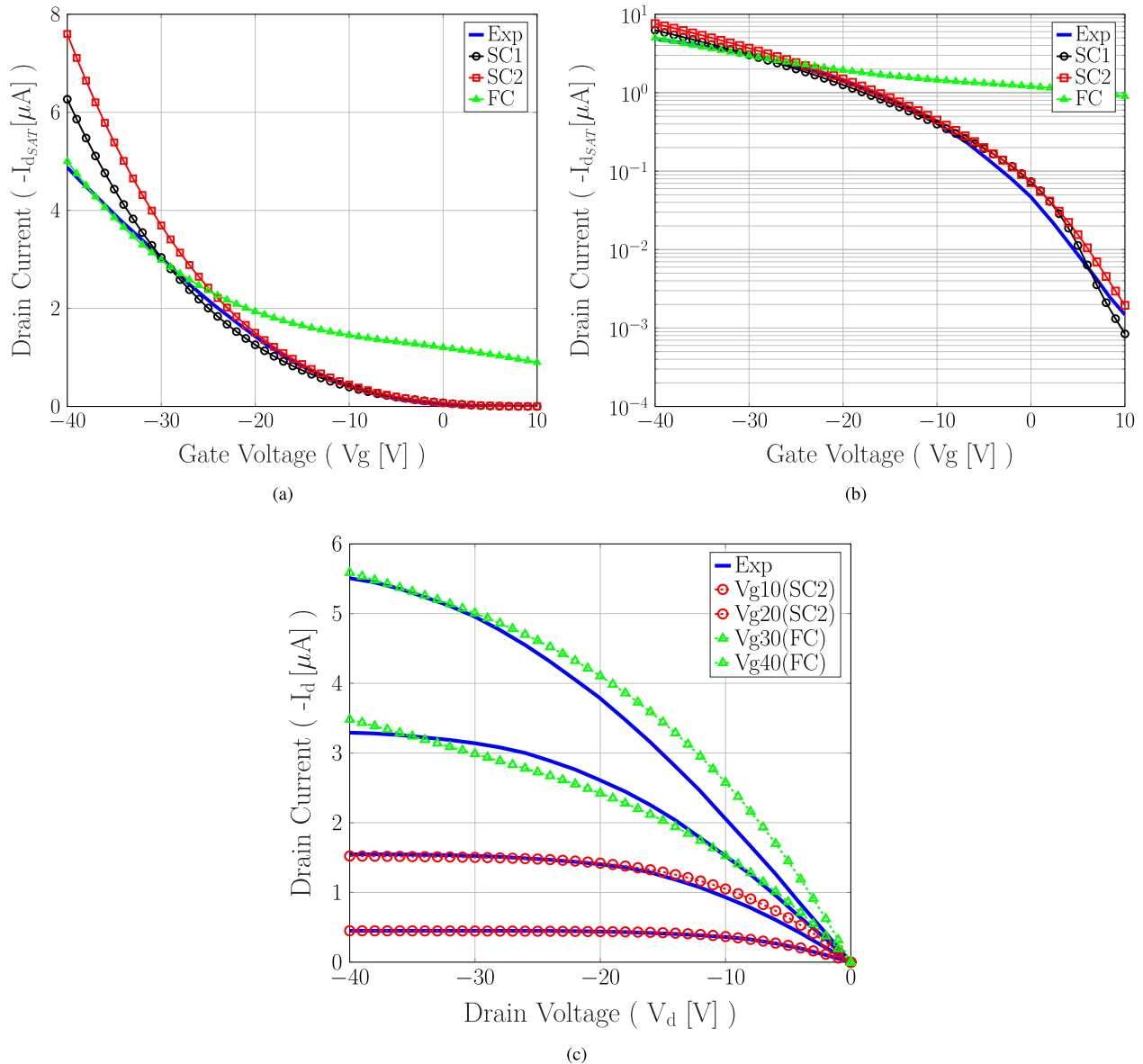
(a)

(b)

(c)

Figure 4. Comparison between DD simulated results and experimental measurements (at $V_d = -30$V) using the fitting scenarios. (a), (b) The fitting of the transfer characteristics both in the linear and logarithmic scales (i.e. for SC1, SC2, and FC). (c) The fitting of the output characteristics using scenarios SC2 and FC.

Table 3. The final set of parameters used under each scenario to fit the experimental transfer characteristics in [74]. All other involved parameters remain unchanged.

	Final simulation parameters				
Scenario	FC	ITH (Energy)	ITE (Energy)	BTH (Energy)	μ_0
SC1	1×10^{19} cm^{-3}	—	5×10^{18} cm^{-3} (0.2 eV)	8×10^{17} cm^{-3} (0.4 eV)	4.62×10^{-4} cm^2 V^{-1} s^{-1}
SC2	4×10^{19} cm^{-3}	6×10^{19} cm^{-3} (0.5 eV)	—	7×10^{18} cm^{-3} (0.3 eV)	4.69×10^{-4} cm^2 V^{-1} s^{-1}
F C	3×10^{19} cm^{-3}	—	—	—	1.65×10^{-4} cm^2 V^{-1} s^{-1}

without the need for any of ITH, ITE, or BTH. The fit corresponding to only using FC is also shown in figure 4.

This approach brought us to the conclusion that the applied gate voltage range is split into two distinct regimes, where the lower regime is described by considering all of FC, ITE (from SC1) or ITH (from SC2), and BTH. While the upper regime is appropriately described using only FC. This conclusion can be further consolidated by looking back at the analysis illustrated

in figure 3. Each of ITE, ITH, BTH only affect the transfer curves substantially in the sub-threshold regime and at low gate voltage in the on-state of our transistor. Possibly, ITH can somehow to a slightly larger extent affect the transfer curves at higher gate voltages compared to the other two, but even if we further increase ITH either in concentration or energy level, we lose any fitting in the lower regime of the gate voltage. At high gate voltages the effect of all three is greatly diminished,
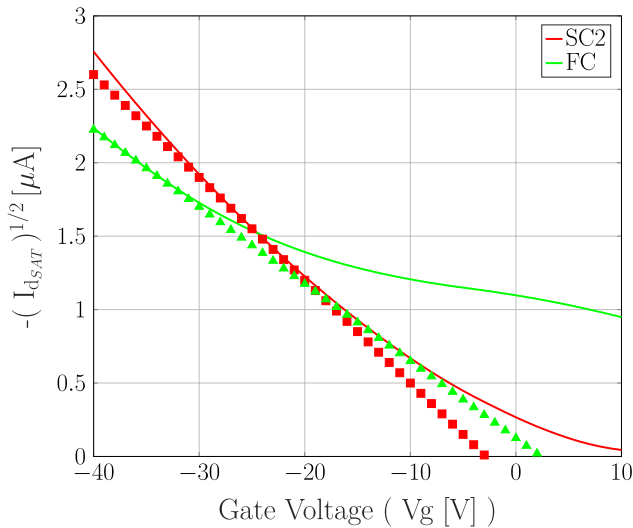
Figure 5. Extracting the threshold voltage V_{th} from the linear fits of the $\sqrt{Id}$ versus Vg relation using parameterizations SC2 and FC.
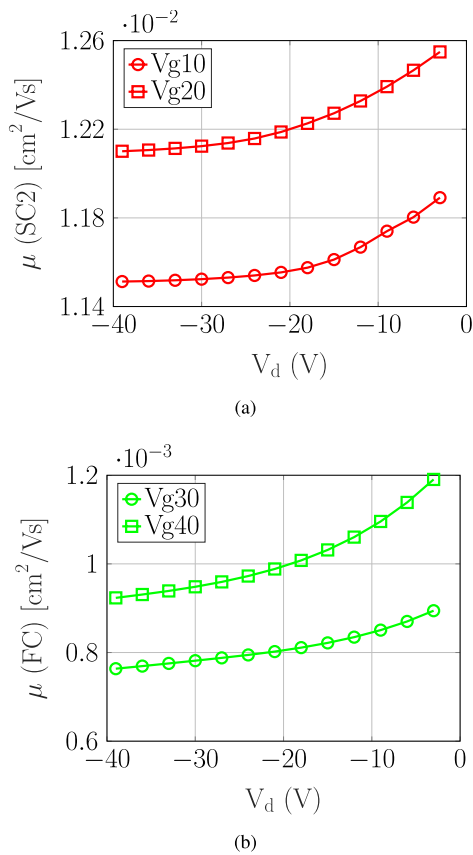

(a)

(b)

Figure 6. Mobility dependence on the drain voltage Vd at different gate voltages Vg, using (a) SC2 and (b) FC.

as all trapped interface and/or bulk charges are freed and join the mobile charges in the channel leading to higher evaluated drain currents. The final simulation parameters used to achieve these fits are summarized in table 3. It is important to note that our starting values for both the trap energies and the μ_0 had to be re-calibrated accordingly to reach our final fits.

After achieving a fit for the transfer curve, we then move on to simulating the output characteristics and once more

draw out a comparison between our simulated results and the experimental measurements. As two scenarios were used for the fitting process (i.e. SC1/SC2 and FC), the same approach is taken for the output characteristics. Between SC1 and SC2, we decided to go forward with the latter to simulate the lower regime of the gate voltage. FC was used to simulate the upper regime respectively. Nevertheless, the reader will find the complete (i.e. covering the entire range) simulated output characteristics for each scenario provided in the supplementary information (see figure (S4)). Final output characteristics using SC2 and FC are depicted in figure 4(c). Quite clearly, with SC2 we successfully reproduced a perfect match for gate voltages of -10V and -20V. Using FC to simulate gate voltages of -30V and -40V did not yield a perfect fit but we were still able to reproduce the correct behaviour in both the linear and saturation regimes as well as the highest evaluated current respectively. Potential profiles across the channel region for the fitted output characteristics are given in figure (S5) of the supplementary information.

3.3. Extracting performance parameters

A crucial part of our investigation, once an agreement is achieved between the simulation and experimental results, we can then extract all important performance parameters of our transistor. These parameters include the V_{th}, and the effective μ of our device. Naturally, based on the results presented in the previous sub-section extracting one value for each is not possible. This is due to the fact that we have two gate voltage regimes described by two different fitting parameterizations. Hence, when coming to extract both V_{th} and μ, this depends on the operating conditions of our device. If it is to be operated at low gate voltages then parameterization SC2 is used, and vise versa FC if the device is operated at high gate voltages. We begin with extracting V_{th}. Figure 5 shows the $\sqrt{Id}$ versus Vg relation. At the lower regime (i.e. using SC2), $V_{th} = -2.8$V, conversely at the higher regime (i.e. using FC) $V_{th} = +2.35$V. The latter coincides with the experimental value. But this difference in V_{th} between high and low operating regimes is a consequence of the fixed charges and/or interface (bulk) traps. In the low regime V_{th} highly depends on the interface and bulk traps, therefore a larger negative voltage is required to switch on the device. In the high regime, it is rather is solely controlled by the fixed charges present and it is shifted towards a more positive value.

A similar approach is taken in extracting the effective μ of our device, and this could easily be done by finding the slope of the linear fits from figure 5. Nevertheless, μ is a rather complex performance parameter that depends on several factors including the temperature, charge density, and the applied voltage (or electric field). We wanted to find it's dependence on the latter, hence we extracted the mobility dependence on the drain voltage (μ versus V_d @ V_g). These dependencies are illustrated in figure 6, and as it can be seen the mobility decreases (rather slightly) as we transition from the linear to the saturation regime of our device. Using SC2, the mobility is between 1.14×10^{-2} cm^2 V^{-1} s^{-1}–1.26×10^{-2} cm^2 V^{-1} s^{-1}, and using

FC it is between $7 \times 10^{-4}\,\mathrm{cm^2\,V^{-1}\,s^{-1}}$–$1.2 \times 10^{-3}\,\mathrm{cm^2\,V^{-1}\,s^{-1}}$. Once again with FC we estimated a mobility closer to the experimental value of $4 \times 10^{-3}\,\mathrm{cm^2\,V^{-1}\,s^{-1}}$.

4. Conclusion

We presented a DD model for the investigation and characterization of OFETs. This model included the GDOS taking into consideration the site density and energetic disorder commonly associated with organic materials, as well as the PF mobility for small molecules (the hopping mobility for polymers). The effects of fixed charges, interface traps and bulk traps (i.e. on the transfer characteristics) were investigated individually. Extending this analysis for the comparison with experimental measurements, we concluded that more than one scenario is required to achieve a good fit depending on the device operating conditions. Eventhough fixed charges are present, the effect of both interface and bulk traps were found to be significant at low gate voltages. Conversely, the current–voltage characteristics are well described with the influence of fixed charges alone at high gate voltages. This was followed by the extraction of transistor performance parameters.

Acknowledgments

ORCID iDs

Mohammed Darwish ⬤ https://orcid.org/0000-0003-0908-0564

References

[1] Lu L, Zheng T, Wu Q, Schneider A M, Zhao D and Yu L 2015 Recent advances in bulk heterojunction polymer solar cells *Chem. Rev.* **115** 12666–731

[2] Yuan J, Gu J, Shi G, Sun J, Wang H Q and Ma W 2016 High efficiency all-polymer tandem solar cells *Nature* **6** 26459

[3] Lui J *et al* 2016 Fast charge separation in a non-fullerene organic solar cell with a small driving force *Nat. Energy* **1** 16089

[4] Nishide J, Nakanotani H, Hiraga Y and Adachi C 2014 High-efficiency white organic light-emitting diodes using thermally activated delayed fluorescence *Appl. Phys. Lett.* **104** 233304

[5] Nakanotani H *et al* 2014 High-efficiency organic light-emitting diodes with fluorescent emitters *Nat. Commun.* **5** 4016

[6] Jou J H, Kumar S, Agrawal A, Li T H and Sahoo S 2015 Approaches for fabricating high efficiency organic light emitting diodes *J. Mater. Chem.* C **3** 2974–3002

[7] Miwa T, Kubo S, Shizu K, Komino T, Adachi C and Kaji H 2017 Blue organic light-emitting diodes realizing external quantum efficiency over 25% using thermally activated delayed fluorescence emitters *Nature* **7** 284

[8] Fei Z *et al* 2014 Influence of side-chain regiochemistry on the transistor performance of high-mobility, all-donor polymers *J. Am. Chem. Soc.* **136** 15154–7

[9] Bronstein H *et al* 2011 Indacenodithiophene-co-benzothiadiazole copolymers for high performance solar cells or transistors via alkyl chain optimization *Macromolecules* **44** 6649–52

[10] Zhang X *et al* 2013 Molecular origin of high field-effect mobility in an indacenodithiophene–benzothiadiazole copolymer *Nat. Commun.* **4** 2238

[11] Yan H *et al* 2009 A high-mobility electron-transporting polymer for printed transistors *Nature* **457** 679–86

[12] Paterson A F *et al* 2018 Recent progress in high-mobility organic transistors: a reality check *Adv. Mater.* **30** 1801079

[13] Uemura T *et al* 2015 On the extraction of charge carrier mobility in high-mobility organic transistors *Adv. Mater.* **28** 151–5

[14] McCulloch I, Salleo A and Chabinyc M 2016 Avoid the kinks when measuring mobility *Science* **352** 1521–2

[15] Bittle E G, Basham J I, Jackson T N, Jurchescu O D and Gundlach D J 2016 Mobility overestimation due to gated contacts in organic field-effect transistors *Nat. Commun.* **7** 10908

[16] Choi H H, Cho K, Frisbie C D, Sirringhaus H and Podzorov V 2018 Critical assessment of charge mobility extraction in FETs *Nat. Mater.* **17** 2–7

[17] Mallik A B *et al* 2007 Design, synthesis, and transistor performance of organic semiconductors *Organic Field-Effect Transistors* ed Z Bao and J Locklin (London: Taylor and Francis) ch 3.1 pp 161–228

[18] Klauk H, Halik M, Zschieschang U, Eder F, Rohde D, Schmid G and Dehm C 2005 Flexible organic complementary circuits *IEEE Electron Devices Soc.* **52** 618–22

[19] Klauk H, Zschieschang U, Pflaum J and Halik M 2007 Ultralow-power organic complementary circuits *Nature* **445** 745–8

[20] Guerin M *et al* 2011 High-gain fully printed organic complementary circuits on flexible plastic foils *IEEE Electron Devices Soc.* **58** 3587–93

[21] Hamaguchi A *et al* 2015 Single-crystal-like organic thin-film transistors fabricated from dinaphtho[2,3-b:2,3-f]thieno[3,2-b]thiophene (DNTT) precursor–polystyrene blends *Adv. Mater.* **27** 6606–11

[22] Niazi M *et al* 2016 Contact-induced nucleation in high-performance bottom-contact organic thin film transistors manufactured by large-area compatible solution processing *Adv. Funct. Mater.* **26** 2371–8

[23] Paterson A F *et al* 2016 Small molecule/polymer blend organic transistors with hole mobility exceeding $13\,\mathrm{cm^2\,V^{-1}\,s^{-1}}$ *Adv. Mater.* **28** 7791–8

[24] Panidi J *et al* 2018 Remarkable enhancement of the hole mobility in several organic small-molecules, polymers, and small-molecule:polymer blend transistors by simple admixing of the lewis acid p-dopant $B(C_6F_5)_3$ *Adv. Sci.* **5** 1700290

[25] Bässler H 1993 Charge transport in disordered organic photoconductors: a monte carlo simulation study *Phys. Status Solidi* B **175** 15–6

[26] Noriega R 2012 Charge transport theories in organic semiconductors *Organic Electronics II: More Materials and Applications* ed H Klauk (New York: Wiley) ch 3, pp 67–104

[27] Podzorov V, Menard E, Borissov A, Kiryukhin V, Rogers J A and Gershenson M E 2004 Intrinsic charge transport on the surface of organic semiconductors *Phys. Rev. Lett.* **93** 086602

[28] Podzorov V, Menard E, Rogers J A and Gershenson M E 2005 Hall effect in the accumulation layers on the surface of organic semiconductors *Phys. Rev. Lett.* **95** 226601

[29] Hasegawa T and Takeya J 2009 Organic field-effect transistors using single crystals *Sci. Technol. Adv. Mater.* **10** 024314

J. Phys. D: Appl. Phys. **53** (2020) 105102

M Darwish and A Gagliardi

[30] Horowitz G 2007 Charge transport in oligomers *Organic Field-Effect Transistors* ed Z Bao and J Locklin (London: Taylor and Francis) ch 2.2, pp 73–99

[31] Stallinga P 2011 Electronic transport in organic materials: comparison of band theory with percolation/(variable range) hopping theory *Adv. Mater.* **23** 3356–62

[32] Troisi A 2011 Charge transport in high mobility molecular semiconductors: classical models and new theories *Chem. Soc. Rev.* **40** 2347–58

[33] der Maur M A, Povolotskyi M, Sacconi F, Pecchia A and Carlo A D 2008 Multiscale simulation of mos systems based on high-κ oxides *J. Comput. Electron.* **7** 398–402

[34] der Maur M A *et al* 2008 Tibercad: towards multiscale simulation of optoelectronic devices *Opt. Quantum Electron.* **40** 1077–83

[35] Gagliardi A, Gentilini D and Carlo A D 2012 Charge transport in solid-state dye-sensitized solar cells *J. Phys. Chem.* C **116** 23882–9

[36] Fallahpour A H *et al* 2014 Optoelectronic simulation and thickness optimization of energetically disordered organic solar cells *J. Comput. Electron.* **13** 933–42

[37] Fallahpour A H *et al* 2014 Modeling and simulation of energetically disordered organic solar cells *J. Appl. Phys.* **116** 184502

[38] Santoni F, Gagliardi A, der Maur M A and Carlo A D 2014 The relevance of correct injection model to simulate electrical properties of organic semiconductors *Org. Electron.* **15** 1557–70

[39] Gagliardi A *et al* 2015 The real TiO2/HTM interface of solid-state dye solar cells: role of trapped states from a multiscale modelling perspective *Nanoscale* **7** 1136–44

[40] Fallahpour A H, Gentilini D, Gagliardi A, der Maur M A, Lugli P and Carlo A D 2016 Systematic study of the PCE and device operation of organic tandem solar cells *IEEE J. Photovolt.* **6** 202–10

[41] Gagliardi A, Wang S and Albes T 2018 Simulation of charge carrier mobility unbalance in organic solar cells *Org. Electron.* **59** 171–6

[42] Darwish M, Boysan H, Liewald C, Nickel B and Gagliardi A 2018 A resistor network simulation model for laser-scanning photo-current microscopy to quantify low conductance regions in organic thin films *Org. Electron.* **62** 474–80

[43] Venkateshvaran D *et al* 2014 Approaching disorder-free transport in high-mobility conjugated polymers *Nature* **515** 384–8

[44] Kaiser W, Albes T and Gagliardi A 2018 Charge carrier mobility of disordered organic semiconductors with correlated energetic and spatial disorder *Phys. Chem. Chem. Phys.* **20** 8897–908

[45] Calhoun M F, Hsieh C and Podzorov V 2007 Effect of interfacial shallow traps on polaron transport at the surface of organic semiconductors *Phys. Rev. Lett.* **98** 096402

[46] Li C, Duan L, Li H and Qiu Y 2014 Universal trap effect in carrier transport of disordered organic semiconductors: transition from shallow trapping to deep trapping *J. Phys. Chem.* C **118** 10651–60

[47] Ucurum C, Goebel H, Yildirim F A, Bauhofer W and Krautschneider W 2008 Hole trap related hysteresis in pentacene field-effect transistors *J. Appl. Phys.* **104** 084501

[48] Zaumseil J and Sirringhaus H 2007 Electron and ambipolar transport in organic field-effect transistors *Chem. Rev.* **107** 1296–323

[49] Sirringhaus H 2009 Reliability of organic field-effect transistors *Adv. Mater.* **21** 3859–73

[50] Bisquert J 2014 *Nanostructured Energy Devices: Equilibrium Concepts and Kinetics* (London: Taylor and Francis) ch 2

[51] Vázquez H, Gao W, Flores F and Kahn A 2005 Energy level alignment at organic heterojunctions: role of the charge neutrality level *Phys. Rev.* B **71** 041306

[52] Linares M *et al* 2010 On the interface dipole at the pentacene-fullerene heterojunction: a theoretical study *J. Phys. Chem.* C **114** 3215–24

[53] Kahn A, Koch N and Gao W 2003 Electronic structure and electrical properties of interfaces between metals and π-conjugated molecular films *J. Polym. Sci.* B **41** 2529–48

[54] Hamadani B H, Corley D A, Ciszek J W, Tour J M and Natelson D 2006 Controlling charge injection in organic field-effect transistors using self-assembled monolayers *Nano Lett.* **6** 1303–6

[55] Morikawa Y, Toyoda K, Hamada I, Yanagisawa S and Lee K 2012 First-principles theoretical study of organic/metal interfaces: vacuum level shifts and interface dipoles *Curr. Appl. Phys.* **12** S2–9

[56] Veres J, Ogier S D, Leeming S W, Cupertino D C and KhaffafF S M 2003 Low-k insulators as the choice of dielectrics in organic field-effect transistors *Adv. Funct. Mater.* **13** 199–204

[57] Kobayashi S *et al* 2004 Control of carrier density by self-assembled monolayers in organic field-effect transistors *Curr. Appl. Phys.* **3** 317–22

[58] Celle C *et al* 2014 Interface dipole: effects on threshold voltage and mobility for both amorphous and poly-crystalline organic field effect transistors *Org. Electron.* **15** 729–37

[59] Nagase T, Hirose T, Kobayashi T, Ueda R, Otomo A and Naito H 2012 Influence of substrate modification with dipole monolayers on the electrical characteristics of short-channel polymer field-effect transistors *Appl. Sci.* **8** 1274

[60] Enengl S *et al* 2016 Spectroscopic characterization of charge carriers of the organic semiconductor quinacridone compared with pentacene during redox reactions *J. Mater. Chem.* C **4** 10265–78

[61] Strakosas X, Bongo M and Owens R M 2015 The organic electrochemical transistor for biological applications *J. Appl. Polym. Sci.* **132** 41735

[62] Zeglio E and Inganäs O 2018 Active materials for organic electrochemical transistors *Adv. Mater.* **30** 1800941

[63] Pasveer W F, Bobbert P A and Michels M A J 2004 Temperature and field dependence of the mobility in 1D for a gaussian density of states *Phys. Status Solidi* C **1** 164–7

[64] Pasveer W F *et al* 2005 Unified description of charge-carrier mobilities in disordered semiconducting polymers *Phys. Rev. Lett.* **94** 206601

[65] Miller A and Abrahams E 1960 Impurity conduction at low concentrations *Phys. Rev.* **120** 745

[66] Meisel K D *et al* 2006 Charge-carrier mobilities in disordered semiconducting polymers: effects of carrier density and electric field *Phys. Status Solidi* C **3** 267–70

[67] Frenkel J 1938 On pre-breakdown phenomena in insulators and electronic semi-conductors *Phys. Rev.* **54** 647

[68] Wang L, Fine D, Basu D and Dodabalapur A 2007 Electric-field-dependent charge transport in organic thin-film transistors *J. Appl. Phys.* **101** 054515

J. Phys. D: Appl. Phys. 53 (2020) 105102

M Darwish and A Gagliardi

[69] Pivrikas A, Ullah M, Sitter H and Sariciftci N S 2011 Electric field dependent activation energy of electron transport in fullerene diodes and field effect transistors: Gill's law *Appl. Phys. Lett.* **98** 092114

[70] Fishchuk I I *et al* 2012 Electric field dependence of charge carrier hopping transport within the random energy landscape in an organic field effect transistor *Phys. Rev.* B **86** 045207

[71] Gill W D 1972 Drift mobilities in amorphous charge-transfer complexes of trinitrofluorenone and poly-n-vinylcarbazole *J. Appl. Phys.* **43** 5033

[72] Ruiz R, Papadimitratos A, Mayer A C and Malliaras G G 2005 Thickness dependence of mobility in pentacene thin-film transistors *Adv. Mater.* **17** 1795–8

[73] Hoppe A, Balster T, Muck T and Wagner V 2008 Scaling limits and MHz operation in thiophene-based field-effect transistors *Phys. Status Solidi* A **205** 612–25

[74] Bolognesi A *et al* 2004 Effects of grain boundaries, field-dependent mobility, and interface trap states on the electrical characteristics of pentacene tft *IEEE Trans. Electron Devices* **51** 1997–2003